Frontiers in Bioscience Landmark

Front. Biosci. (Landmark Ed) **2026**; 31(10): 53084
https://doi.org/10.31083/FBL53084

Original Research

FTO Promotes Osteosarcoma Progression via *YAP* and Reduces Cisplatin Sensitivity

Zhaoliang Shen[1], Fei Li[1], Zhihao Chen[1], Yuxing Zhang[2], Xiaoqian Dang[1,*], Haoyu Wang[1,*]

[1]Department of Orthopedics, The Second Affiliated Hospital of Xi'an Jiaotong University, 710004 Xi'an, Shaanxi, China
[2]Medical College, Xijing University, 710123 Xi'an, Shaanxi, China
*Correspondence: dangxiaoqian@mail.xjtu.edu.cn (Xiaoqian Dang); surgeonwanghaoyu@mail.xjtu.edu.cn (Haoyu Wang)
Academic Editor: Elisa Belluzzi
Submitted: 19 April 2026 Revised: 2 August 2026 Accepted: 24 August 2026 Published: 15 October 2026

Abstract

Background: Fat mass and obesity-associated protein (*FTO*), a key demethylase involved in N6-methyladenosine modification, plays significant regulatory roles in various cancers. However, its influence on osteosarcoma progression, sensitivity to the commonly used chemotherapy agent cisplatin, and downstream regulatory mechanisms remain unclear. **Methods:** Multiple osteosarcoma cell lines were used for expression and drug-sensitivity screening, with MG-63 selected for mechanistic experiments. Genetically modified cell lines were established via viral infection and transfection. *In vitro* assays, including CCK-8, colony formation, Transwell, wound healing, and flow cytometry, were used to assess cell proliferation, migration, and cisplatin sensitivity. Subcutaneous xenograft and tail vein injection metastasis models were used to evaluate *in vivo* tumor growth and metastasis. Transcriptome sequencing was performed to identify downstream target genes. **Results:** Compared to normal osteoblasts, FTO expression was elevated in osteosarcoma cell lines ($p < 0.05$). Knockdown of *FTO* inhibited osteosarcoma cell proliferation and migration, reduced tumor growth and metastasis *in vivo*, and increased sensitivity to cisplatin (all $p < 0.01$). In contrast, overexpression of *FTO* produced the opposite effects (all $p < 0.05$). Yes-associated protein (*YAP*) was identified as a downstream target of *FTO*. Overexpression of *YAP* rescued the tumor-suppressive effects caused by *FTO* knockdown (all $p < 0.01$), whereas *YAP* knockdown attenuated the tumor-promoting functions of *FTO* overexpression (all $p < 0.05$). **Conclusions:** *FTO* is overexpressed in osteosarcoma, where it promotes tumor progression and reduces cisplatin sensitivity. *YAP*, as a downstream target of FTO, mediates the oncogenic functions of FTO.

Keywords: osteosarcoma; N6-methyladenosine; alpha-ketoglutarate-dependent dioxygenase FTO; YAP-signaling proteins; antineoplastic agents

1. Introduction

Osteosarcoma is the most common malignant bone tumor, originating from mesenchymal cells, and is frequently observed in the pediatric and adolescent population [1]. Although surgical intervention combined with adjuvant chemotherapy has significantly improved the five-year survival rate for osteosarcoma patients, resistance to standard chemotherapeutic drugs like cisplatin often leads to poor prognosis [2]. Despite the identification of numerous genes that play crucial regulatory roles in the initiation, progression, and chemoresistance of osteosarcoma [3,4], elucidating the molecular mechanisms underlying osteosarcoma development and identifying the causes of chemoresistance remain challenging, hindering the development of newer, more targeted, and more effective therapies.

N6-methyladenosine (m^6A) modification, a type of epitranscriptomic modification, is the most widespread post-transcriptional modification in eukaryotes [5]. A methyltransferase complex composed of multiple subunits mediates m^6A modification, while demethylases, including fat mass and obesity-associated protein (*FTO*), remove methyl groups from RNA to achieve controlled reversible regulation [6]. As the first m^6A demethylase discovered, *FTO* plays key roles in physiological processes such as embryonic development and organ formation [7], as well as in diseases such as diabetes [8] and obesity [9]. In cancer, various studies have identified dysregulation of *FTO* expression, highlighting its critical importance in tumor progression in various malignancies such as breast cancer [10], glioblastoma [11], cervical cancer [12], and melanoma [13]. However, the role of *FTO* in osteosarcoma remains underexplored, and its specific mechanisms are unclear.

The Hippo pathway represents an evolutionarily conserved signaling mechanism that regulates cell proliferation, apoptosis, and stem cell renewal. As a primary effector of the Hippo pathway, Yes-associated protein (*YAP*) acts as a transcription factor to promote cell proliferation and inhibit apoptosis [14,15]. Previous studies have established the cancer-promoting role of *YAP* in osteosarcoma [16,17], but its upstream regulatory mechanisms, particularly at the epigenetic level, are not fully understood.

Emerging evidence suggests a potential functional interplay between m^6A modification and Hippo/*YAP* signaling in cancer. Notably, the *FTO*/*YAP* axis has been impli-

Copyright: © 2026 The Author(s). Published by IMR Press.
This is an open access article under the CC BY 4.0 license.

Publisher's Note: IMR Press stays neutral with regard to jurisdictional claims in published maps and institutional affiliations.

cated in chemoresistance in certain cancer types [18], however, whether *FTO* directly regulates *YAP* in osteosarcoma and whether this regulation contributes to osteosarcoma progression and cisplatin sensitivity have not been fully explained. This study investigates the role of *FTO* in osteosarcoma proliferation, migration, invasion, and cisplatin sensitivity, both *in vitro* and *in vivo*, as well as FTO's regulatory function on *YAP* expression. Furthermore, the study reveals that *FTO* exerts cancer-promoting effects through *YAP*-dependent mechanisms, providing new insights into the *FTO/YAP* regulatory axis in osteosarcoma and highlighting potential therapeutic targets.

2. Materials and Methods

2.1 Cell Culture and Infection

The human osteoblast cell line hFOB1.19 (ZQ0402, Zhong Qiao Xin Zhou Biotechnology, Shanghai, China), was cultured in DMEM/F12 medium (PM150312, Procell, Wuhan, Hubei, China). The human osteosarcoma cell lines HOS (CL-0360, Procell, Wuhan, Hubei, China), and MG-63 (CL-0157, Procell, Wuhan, Hubei, China) were cultured in MEM (PM150411, Procell, Wuhan, Hubei, China), and U-2OS (CL-0236, Procell, Wuhan, Hubei, China) and Saos-2 (CL-0202, Procell, Wuhan, Hubei, China) were cultured in McCoy's 5A (PM150710, Procell, Wuhan, Hubei, China). All cell culture media were supplemented with 10% FBS (16000044, Thermo Fisher Scientific, Waltham, MA, USA) and penicillin/streptomycin (ST488S, Beyotime, Shanghai, China). Cells were cultured at 37 °C in a 5% CO_2 environment, except for hFOB1.19 cells, which were maintained at 33.5 °C. All cell lines were authenticated by short tandem repeat (STR) profiling and confirmed to be free of mycoplasma contamination.

As cell lines with extremely high or low basal FTO expression may not adequately reveal phenotypic changes following bidirectional modulation, MG-63, with moderate FTO expression, was selected for mechanistic studies. For viral infection, cells were seeded and then incubated with viral particles, and 5 µg/mL polybrene (Hanbio, Shanghai, China) at concentrations determined by the viral titer and multiplicity of infection (MOI). After 24 h of infection, the medium was replaced, and the corresponding selection agent was applied for screening.

Cells for transfection were serum-starved for 12 hours after reaching about 50% confluence. 100 pmol siRNA was mixed with 5 µL Lipofectamine 2000 transfection reagent (Thermo Fisher Scientific, Waltham, MA, USA) and added to the culture medium. After 8 h, the medium was replaced with complete medium. Transfection efficiency was evaluated by quantitative polymerase chain reaction (qPCR) at 48 h post-transfection.

The *FTO* knockdown lentivirus (Vector: pHBLV-U6-shRNA-puromycin-ZsGreen) was obtained from Hanbio Company (Shanghai, China). *YAP* and *FTO* overexpression lentiviruses (Vector: ubi-MCS-puromycin-GFP) were from GeneChem Company (Shanghai, China). Sangon Biotech (Shanghai, China) synthesized siRNA. All the knockdown sequences are listed in **Supplementary Table 1**.

For lentiviral transduction, cells were seeded in 6-well plate at a density of 1×10^5 cells per well and infected with lentivirus at a multiplicity of infection (MOI) of 50 in the presence of polybrene (5 µg/mL, Hanbio Company, Shanghai, China). After 24 h, the virus-containing medium was replaced with fresh complete medium. At 48 h post-infection, selection was initiated with puromycin (2 µg/mL, MedChemExpress, Monmouth Junction, NJ, USA) for 14 days until uninfected control cells were completely eliminated. Transduction efficiency was confirmed by fluorescence microscopy qPCR.

2.2 Bioinformatics and Database Analysis

Pan-cancer expression of *FTO* and *YAP* was analyzed using the "Pan-cancer box plot" module of the TNMplot web tool (https://tnmplot.com/analysis/) [19], with default settings comparing tumor and normal tissues across all available cancer types. The expression difference between osteosarcoma and normal bone tissue was assessed using the "Multi-gene analysis" module of the same tool. Survival analyses for *FTO* and *YAP* were conducted using GEPIA (http://gepia.cancer-pku.cn/) [20], employing the median expression value as the group cutoff. Overall survival and disease-free survival curves were generated, and hazard ratios with 95% confidence intervals were calculated. The gene-gene correlation between *FTO* and *YAP* was also analyzed using the correlation module of GEPIA. To identify putative m^6A modification sites, the *YAP* mRNA sequence was submitted to the SRAMP prediction server (http://www.cuilab.cn/sramp/) [21] with default settings. Experimental evidence for the binding of FTO to *YAP* mRNA was retrieved from the RM2Target database (http://rm2target.canceromics.org/) [22], which integrates published CLIP-seq and eCLIP-seq data.

2.3 RNA Extraction and qPCR

Total RNA was extracted using the TRIzol method (Thermo Fisher Scientific, Waltham, MA, USA) and quantified using NanoDrop One Micro-Spectrophotometer (Thermo Fisher Scientific, Waltham, MA, USA). 1 µg RNA was reverse-transcribed into cDNA using a reverse transcription kit (AG11711, Accurate Biology, Changsha, Hunan, China). Target RNA quantification was performed using qPCR reagents (AG11702, Accurate Biology, Changsha, Hunan, China) on LightCycler 480 (Roche, Basel, CH). Primer sequences are listed in **Supplementary Table 1**. The target gene expression was normalized to *ACTB* as the endogenous reference. For experiments with a designated control group, relative quantification was calculated using the $2^{-\Delta\Delta Ct}$ method; for experiments without a control group, the $2^{-\Delta Ct}$ method was applied. All reactions were performed in triplicate technical replicates, and data were obtained from at least 3 independent biological replicates.

2.4 Western Blot

Cells were washed with PBS, then lysed in RIPA lysis buffer (P0013B, Beyotime, Shanghai, China). Lysate was then centrifuged, and loading buffer was added before boiling. Equal amounts of total protein (20 μg per lane) were loaded onto 10% SDS-PAGE, electrophoresed, and then transferred onto PVDF membranes (Millipore, Darmstadt, DE). The membranes were blocked with 5% non-fat milk in TBST for 1 h at room temperature. Subsequently, the sections were sequentially incubated with primary antibodies diluted in antibody dilution buffer (P0256, Beyotime, Shanghai, China) overnight at 4 °C. Primary antibodies and their working dilutions are as follows: *FTO* Rabbit mAb (45980, Cell Signaling Technology, Danvers, MA, USA, 1:1000), E-cadherin Rabbit mAb (3195, Cell Signaling Technology, USA, Danvers, MA, 1:1000), N-cadherin Rabbit mAb (13116, Cell Signaling Technology, Danvers, MA, USA, 1:1000), Vimentin Rabbit mAb (5741, Cell Signaling Technology, Danvers, MA, USA, 1:1000), *YAP* Rabbit mAb (14074, Cell Signaling Technology, Danvers, MA, USA, 1:1000), GAPDH Rabbit mAb (2118, Cell Signaling Technology, Danvers, MA, USA, 1:1000), beta-Actin Rabbit mAb (4970, Cell Signaling Technology, Danvers, MA, USA, 1:1000). After washing with TBST, the membranes were incubated with HRP-linked anti-rabbit antibodies (7074, Cell Signaling Technology, Danvers, MA, USA, 1:5000) for 1 h at room temperature. Immunoreactive bands were visualized using ECL substrate (Epizyme, Shanghai, China) and imaged with a chemiluminescence imaging system (Tanon, Shanghai, China). Densitometric analysis was performed using ImageJ software (version 1.54m, National Institutes of Health, Bethesda, MD, USA). Relative protein levels were normalized to the internal control. All experiments were independently repeated at least 3 times.

2.5 Cell Proliferation Assay and Plate Colony Formation Assay

CCK-8: The assay was used to detect cell proliferation. Briefly, cells were seeded in 96-well plates at a density of 5×10^3 cells per well. After adhesion, at 0, 24, 48, 72, 96, and 120 h, the medium was replaced, and 10% CCK-8 solution (HY-K0301, MedChemExpress, Monmouth Junction, NJ, USA) was added. After further incubation for 2 h, the absorbance at 450 nm was measured using a microplate reader (Agilent, Santa Clara, CA, USA). Each time point was assayed in quintuplicate wells, and the entire experiment was independently repeated three times. The absorbance values were plotted against time to generate proliferation curves.

For the plate colony formation assay, cells were seeded at a density of 200 cells/well in a 6-well plates and cultured for 10 days. After cell clusters consisting of more than 50 cells formed, cells were washed with PBS (Servicebio, Wuhan, Hubei, China), fixed with 4% paraformaldehyde (P0099, Beyotime, Shanghai, China), stained with crystal violet (C0121, Beyotime, Shanghai, China), photographed, and the number of colonies was counted. Each group was assayed in triplicate wells, and the entire experiment was independently repeated three times.

2.6 Wound Healing Assay

5×10^5 cells per well were seeded into 6-well plates and grown to 90% confluency. A straight wound was created by scratching the monolayer with a sterile pipette tip. Detached cells were removed by washing with PBS, and images were captured at 0 h under a microscope. After 48 h of incubation in serum-free medium, the cells were washed again with PBS, and images were taken under a microscope. Then the percentage of wound healing was calculated. Three replicate wells were set up for each group, and the experiment was independently repeated three times.

2.7 Transwell Assay

After 12 h of starvation, cells were resuspended in serum-free medium and seeded into 8-μm pore Transwell chambers (Corning, Corning, NY, USA) at a density of 10^4 cells/chamber, with complete medium added to the lower chamber as a chemoattractant. After 24 h of culture, cells on the membrane surface were removed. The chambers were then washed with PBS, fixed with 4% paraformaldehyde, stained with crystal violet, and washed. Images were captured, and the cells that had migrated through the membrane were counted. Five replicate wells were set up for each group, and the experiment was independently repeated three times.

2.8 Flow Cytometry for Apoptosis Detection

Cells were harvested, washed with PBS, centrifuged, and resuspended in Annexin V binding buffer (BioLegend, San Diego, CA, USA). Annexin V-FITC was then added, and the mixture was incubated on ice in the dark for 15 minutes. Five minutes before the end of the incubation, PI solution was added. Following incubation, cells were analyzed by flow cytometry (Beckman Coulter, Miami, FL, USA). Data acquisition and analysis were performed using the instrument's built-in CytExpert software (Beckman Coulter, Miami, FL, USA). After excluding debris and doublet cells, four-quadrant gating thresholds were established by reference to unstained and single-stained control samples. Early apoptotic cells were defined as Annexin V^+/PI^- (Q3), late apoptotic cells as Annexin V^+/PI^+ (Q2), and necrotic cells as Annexin V^-/PI^+ (Q1). The total apoptosis rate was calculated as the sum of the percentages of early and late apoptotic cells. Three independent experiments were conducted.

2.9 Drug Sensitivity Assay

For cisplatin sensitivity assays, 2×10^4 cells per well were seeded into 96-well plates. After cell attachment, the cells were treated with cisplatin (HY-17394, MedChemExpress, Monmouth Junction, NJ, USA) dissolved in 0.9%

sterile NaCl to prepare a stock solution of 1 mg/mL, which was stored at –80 °C and protected from light. Working solutions were freshly prepared by diluting the stock in culture medium immediately before use to final concentrations of 0, 0.25, 0.5, 1, 2.5, 5, 10, and 20 μg/mL. And cells were incubated with cisplatin for 24 h. The medium was then replaced, and CCK-8 solution (HY-K0301, MedChemExpress, Monmouth Junction, NJ, USA) was added at 1/10 medium volume. After 2 h of incubation, the absorbance at 450 nm was measured. Cell viability was calculated as a percentage of the untreated control. Dose–response curves were fitted by using a four-parameter nonlinear regression model and the IC_{50} value was derived from the fitted curves. Each concentration was assayed in quintuplicate wells, and the experiment was independently repeated three times. IC_{50} values obtained from independent experiments were compared between groups.

2.10 Xenograft Tumor Model

A total of 80 six-week-old male BALB/c nude mice were purchased from the Experimental Animal Center of Xi'an Jiaotong University and raised in an SPF environment with a temperature of 21 °C, humidity at 55%, and a 12 h/12 h light/dark cycle. The individual mouse was considered the experimental unit. Based on our previous experimental experience and established protocols, 5 mice per group were considered sufficient to detect consistent and reproducible differences in tumor growth and metastasis, while complying with the 3R principles to minimize animal use. Mice that failed to develop tumors or died unexpectedly before the endpoint were excluded from the analysis; only mice that developed palpable tumors and survived to the predefined endpoint were included.

For subcutaneous tumorigenesis, MG-63 cells grown to 80% confluence were harvested and resuspended in PBS to a density of 10^7 cells/mL. Mice were randomly assigned to groups (n = 5 per group) using a random number generator. Mouse anesthesia was induced with 3% isoflurane in 100% oxygen at a flow rate of 1 L/min in an induction chamber and maintained with 2% isoflurane via a nose cone. After the loss of the pedal withdrawal reflex, the backs of each nude mouse were disinfected, and 100 μL of cell suspension was injected subcutaneously. When spherical or oval tumors became visible, tumor volume was measured using a digital caliper on days 7, 14, 21, and 28. The experimental endpoint was predefined as day 28 after tumor cell inoculation. If a tumor reached 2000 mm^3 or the animal showed signs of severe distress before day 28, the animal was euthanized immediately. Tumor measurement was performed by an investigator blind to group allocation and tumor volume was calculated as $V = (Length \times Width^2) / 2$. Mice were then euthanized by cervical dislocation following deep isoflurane anesthesia with 5% isoflurane in 100% oxygen at a flow rate of 1 L/min. Tumors were harvested, fixed, and imaged.

To establish a lung metastasis model, mice were randomly assigned to groups (n = 5 per group) and 3×10^6 osteosarcoma MG-63 cells were injected into the tail veins of BALB/c nude mice without anesthesia. Mice were routinely raised for 4 weeks and euthanized by cervical dislocation under deep isoflurane anesthesia with 5% isoflurane in 100% oxygen at a flow rate of 1 L/min. Lung tissue was harvested to observe and count the pulmonary metastatic nodules. Obtained tissue was fixed, sectioned, and stained with hematoxylin and eosin (H&E). Metastatic burden was quantified as the percentage of tumor area relative to total area, with the scorer blinded to group allocation. Randomization and group allocation were performed by an independent investigator not involved in tumor measurement or scoring, and the blinding code was not revealed until all measurements and analyses were completed.

All animal procedures were conducted in accordance with the Guide for the Care and Use of Laboratory Animals and were approved by the Institutional Animal Care and Use Committee (IACUC) of the Laboratory Animal Research Center of Xi'an Jiaotong University, under approval number: XJTUAE20253836.

2.11 Immunohistochemistry (IHC)

Harvested tumor tissue was washed with PBS, fixed with 4% paraformaldehyde, and embedded in paraffin for sectioning. Sections were baked, deparaffinized, rehydrated, and subjected to antigen retrieval. After permeabilization with 0.3% Triton-X-100 and blocking with 5% goat serum, sections were incubated overnight at 4 °C with anti-Ki67 antibody (28074-1-AP, Proteintech, Wuhan, Hubei, China, 1:2000). The sections were then washed and incubated with HRP-conjugated secondary antibody (RGAR011, Proteintech, Wuhan, Hubei, China, ready-to-use) for 1 h at room temperature. Immunoreactivity was visualized with DAB, followed by counterstaining with hematoxylin. The stained sections were imaged under a microscope.

Human osteosarcoma tissue microarray was commercially purchased from Xi'an Zhongke Guanghua Bioaitech Co., Ltd. (L714901, Xi'an, Shaanxi, China). IHC staining for FTO was performed using the same protocol with anti-FTO antibody (27226-1-AP, Proteintech, Wuhan, Hubei, China, 1:400) and HRP-conjugated secondary antibody (RGAR011, Proteintech, Wuhan, Hubei, China, ready-to-use). Stained sections were photographed, and the percentage of FTO-positive cells was quantified using ImageJ software. Based on the median percentage of FTO-positive cells, samples were classified into two groups: FTO-high expression and FTO-low expression. The relation between FTO expression and the sample characteristics was analyzed using a chi-square test.

2.12 RNA Immunoprecipitation (RIP)-PCR

Cells were harvested and lysed in cell lysis buffer (P0013, Beyotime, Shanghai, China) supplemented with protease inhibitor cocktail (P8340, Sigma-Aldrich) and RNase inhibitor (HY-K1033, MedChemExpress, Monmouth Junction, NJ, USA) for 30 min on ice. The lysate was centrifuged at 12,000 ×g for 15 min at 4 °C, and the supernatant was collected. 1/10 of the lysate was saved as "input" for RNA quantification. The remaining lysate was divided equally and incubated overnight at 4 °C with 5 µg of anti-FTO antibody (45980, Cell Signaling Technology, Danvers, MA, USA) or an equal amount of normal rabbit IgG (2729, Cell Signaling Technology, Danvers, MA, USA) as negative control, with gentle rotation. Protein A/G magnetic beads (HY-K0202, MedChemExpress, Danvers, MA, USA) were pre-washed with wash buffer and then added to the antibody-lysate mixture for an additional 2 h incubation at 4 °C. After incubation, the beads were collected on a magnetic rack and washed with cold wash buffer. RNA was purified from both the immunoprecipitated samples and the input using TRIzol reagent (Thermo Fisher Scientific, Waltham, MA, USA). Reverse transcription was performed with a reverse transcription kit (AG11711, Accurate Biology, Changsha, Hunan, China). And cDNA was subjected to conventional PCR using PCR reagents (AG11007, Accurate Biology, Changsha, Hunan, China) over a total of 25 cycles. Primers were designed to flank the m^{6}A sites with the highest confidence score in the *YAP* mRNA predicted by SRAMP and to amplify an 80–150 bp product containing the target adenine within the amplification region. The primer sequences are listed in **Supplementary Table 1**. PCR products were loaded on a 2% agarose gel stained with nucleic acid gel stain (10201ES03, Yeasen Biotechnology, Shanghai, China) added and visualized using a gel imaging system (1600T, Tanon, Shanghai, China). All experiments were independently repeated at least three times.

2.13 Methylated RNA Immunoprecipitation (MeRIP)-qPCR

Total RNA was extracted using TRIzol reagent (Thermo Fisher Scientific, Waltham, MA, USA). MeRIP was performed using the riboMeRIP m^{6}A Kit (C11051-1, Ribobio, Guangzhou, Guangdong, China) according to the manufacturer's instructions. Briefly, total RNA was chemically fragmented using RNA fragmentation reagent at 70 °C for 7 min. 1/10 of the fragmented RNA was saved as "input". Magnetic beads A/G were then incubated with 5 µg of anti-m^{6}A antibody or normal mouse IgG (68860, Cell Signaling Technology, Danvers, MA, USA) for 30 min under rotation. After washing three times, the fragmented RNA was subjected to immunoprecipitation with m^{6}A antibody or IgG-conjugated beads for 2 h at 4 °C. The beads were washed three times with wash buffer, and the bound RNA was eluted with elution buffer. RNA from both the immunoprecipitated and input fractions was purified by phenol-chloroform extraction and ethanol precipitation. cDNA synthesis and qPCR were performed as described above, using primers flanking the high-confidence m^{6}A sites on *YAP* mRNA predicted by SRAMP. The m^{6}A enrichment level was determined by normalizing the qPCR signal of the m^{6}A-IP to the input (ΔCt). All reactions were performed in triplicate technical replicates, and data were obtained from at least 3 independent biological replicates.

2.14 Statistical Analysis

All cell-based experiments were performed in three independent replicates, and the data were expressed as mean ± SD. For animal experiments, a single cohort of n = 5 mice per group was used. Data from animal experiments are presented as the mean ± SD. ImageJ software (version 1.54m, National Institutes of Health, Bethesda, MD, USA) was used for image analysis. GraphPad Prism software (version 9.3.0, GraphPad Software, Boston, Massachusetts, USA) was used for statistical analysis and graphing. Data distribution was assessed for normality using the Shapiro–Wilk test, and homogeneity of variances was verified using Levene's test. For two-group comparisons, an unpaired Student's *t*-test was applied. For comparisons among more than two groups, one-way ANOVA was used, followed by Dunnett's test for comparisons against a common control. For repeated measures, two-way ANOVA was performed. All statistical tests were two-sided, and a p value less than 0.05 was considered statistically significant.

3. Results

3.1 FTO Is Highly Expressed in Osteosarcoma

Analysis of *FTO* expression across various cancer types using TNMplot [19] indicated that *FTO* was upregulated in multiple malignancies including acute myeloid leukemia (AML), colorectal cancer, liver cancer, small cell lung cancer, ovarian cancer, pancreatic cancer, clear cell renal carcinoma, skin cancer, stomach cancer and thyroid carcinoma (Fig. 1A). Furthermore, the *FTO* expression in osteosarcoma was significantly increased compared to normal tissue (Fig. 1B). Survival analysis via GEPIA [20] suggested that high *FTO* expression was negatively correlated with overall survival and disease-free survival (Fig. 1C,D). Subsequently, to verify altered *FTO* expression in osteosarcoma, osteosarcoma cells, including MG-63, Saos-2, HOS, U-2OS, and normal bone cell line hFOB1.19, were established. qPCR results showed that *FTO* expression was significantly elevated in osteosarcoma cells compared to bone cells (Fig. 1E), with immunoblotting further confirming this upregulation at the protein level (Fig. 1F). Among all these cell lines, MG-63 exhibited moderate endogenous *FTO* expression at both the mRNA and protein levels, making it suitable for further knockdown and overexpression. Additionally, IHC staining of FTO on an osteosarcoma tissue microarray revealed that among 70 os-

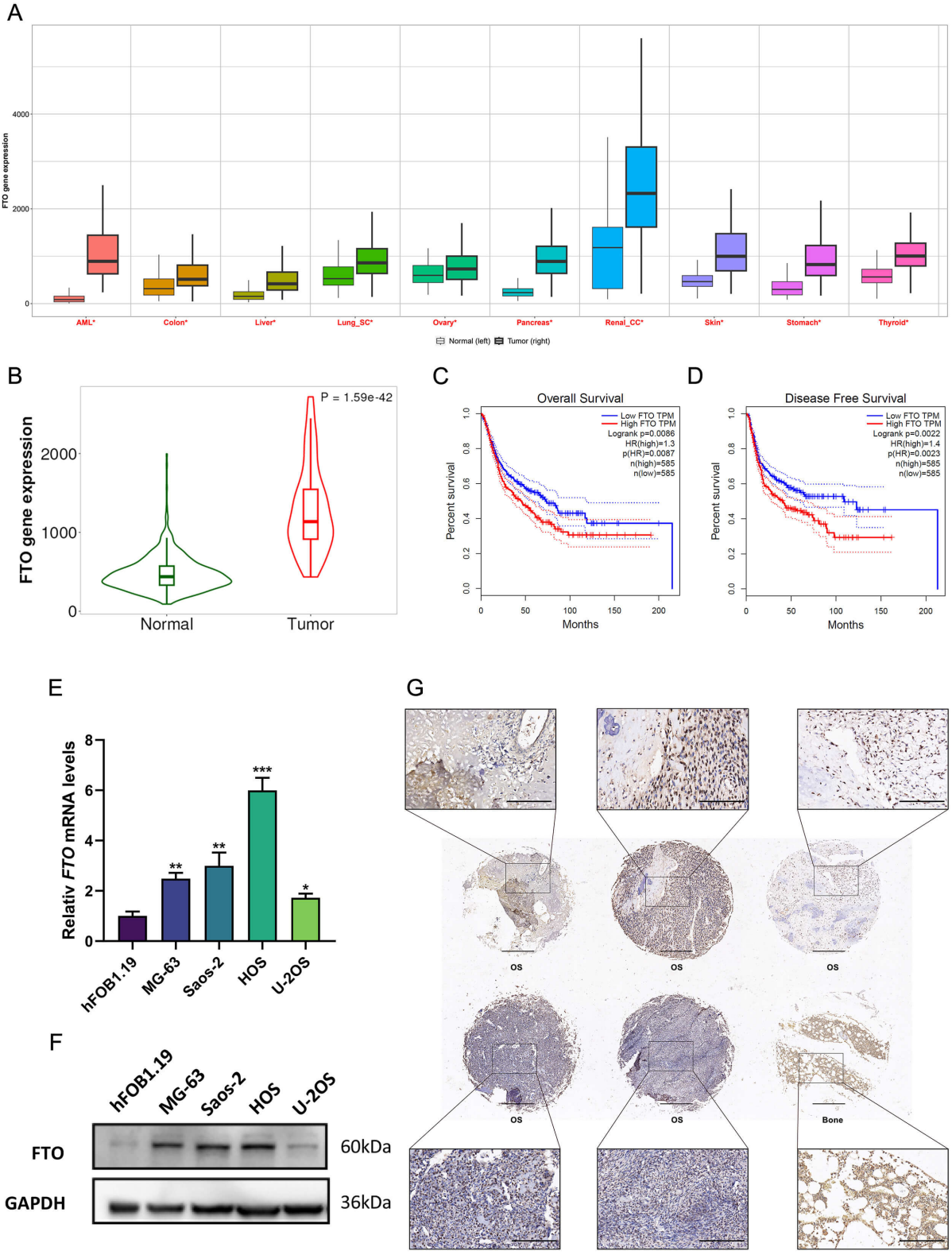


Fig. 1. FTO is highly expressed in osteosarcoma. (A) Expression of FTO in multiple types of cancer versus normal controls. Red labels indicate statistically significant differences. (B) Expression of FTO in osteosarcoma versus normal bone tissue. (C,D) Kaplan-Meier analysis of overall survival (C) and disease-free survival (D) in cancer patients based on FTO expression. (E,F) FTO mRNA (E) and protein (F) levels in human osteoblast cell lines and osteosarcoma cell lines. GAPDH was used as an internal reference. (G) Immunohistochemical staining of FTO protein in osteosarcoma microarray. Scale bar: 500 μm for the overview images; 200 μm for the magnified images. $^{*}p < 0.05$; $^{**}p < 0.01$; $^{***}p < 0.001$. FTO, fat mass and obesity-associated protein.

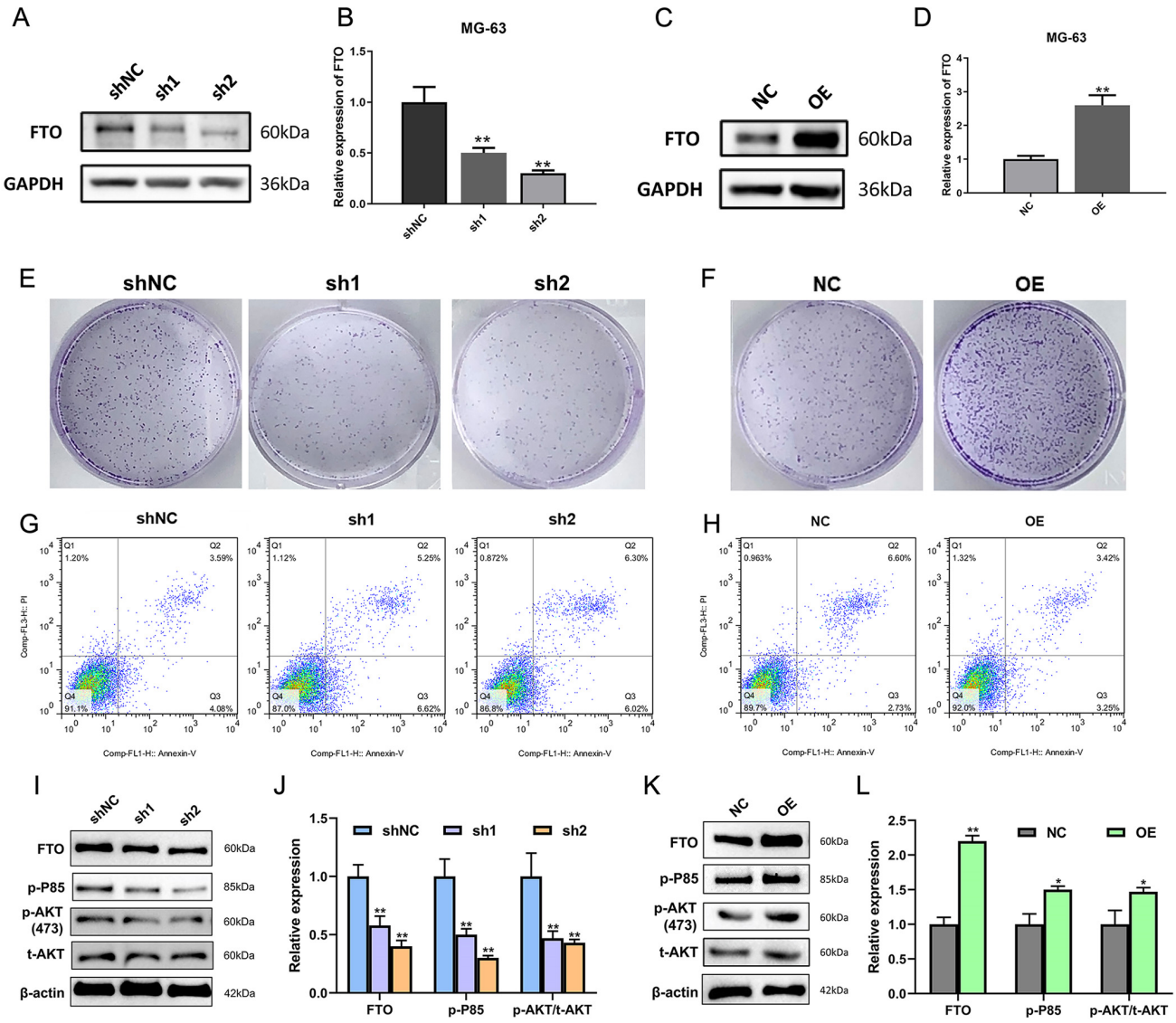


Fig. 2. FTO promotes osteosarcoma cell proliferation *in vitro*. (A–D) Western blot validation of FTO knockdown (A,B) and overexpression (C,D) in MG-63 cells. GAPDH was used as a reference. (E,F) Colony formation assay in MG-63 cells with FTO knockdown (E) or overexpression (F). (G,H) Flow cytometry analysis of apoptotic cell ratios in MG-63 cells with FTO knockdown (G) or overexpression (H). (I–L) Western blot showing PI3K-Akt pathway-related protein and phosphorylation levels in FTO knockdown (I,J) or overexpression (K,L) MG-63 cells. β-actin was used as an internal reference. $^{*}p < 0.05$, $^{**}p < 0.01$.

teosarcoma samples, *FTO* expression showed no significant correlation with patient gender, age, or TNM stage, but was positively correlated with lymph node metastasis (Fig. 1G and **Supplementary Table 2**). Thus, *FTO* expression is elevated in osteosarcoma and correlates with poor prognosis.

3.2 FTO Promotes Osteosarcoma Progression and Suppresses Cisplatin Sensitivity In Vitro

To verify the role of *FTO* in osteosarcoma progression, MG-63 cells, which displayed intermediate endogenous *FTO* expression, were selected to establish *FTO* knockdown and overexpression cell lines. The efficiency of knockdown and overexpression was verified by immunoblotting (Fig. 2A–D). Colony formation assay suggested that knockdown of *FTO* inhibited the colony formation, whereas *FTO* overexpression promoted it, suggesting that *FTO* promotes osteosarcoma cell proliferation (Fig. 2E,F and **Supplementary Fig. 1A,B**). Flow cytometry revealed that *FTO* knockdown increased the proportion of apoptotic osteosarcoma cells, while *FTO* overexpression suppressed apoptosis (Fig. 2G,H and **Supplementary Fig. 1C,D**). Immunoblotting showed that *FTO* knockdown was accompanied by reduced p-p85 levels and decreased phosphorylation of Akt at S473, whereas *FTO* overexpression led to the opposite pattern (Fig. 2I–L). These changes in PI3K-Akt phosphorylation are consistent with the observed alterations in cell proliferation, suggesting that FTO may positively modulate the activity of this pathway. How-

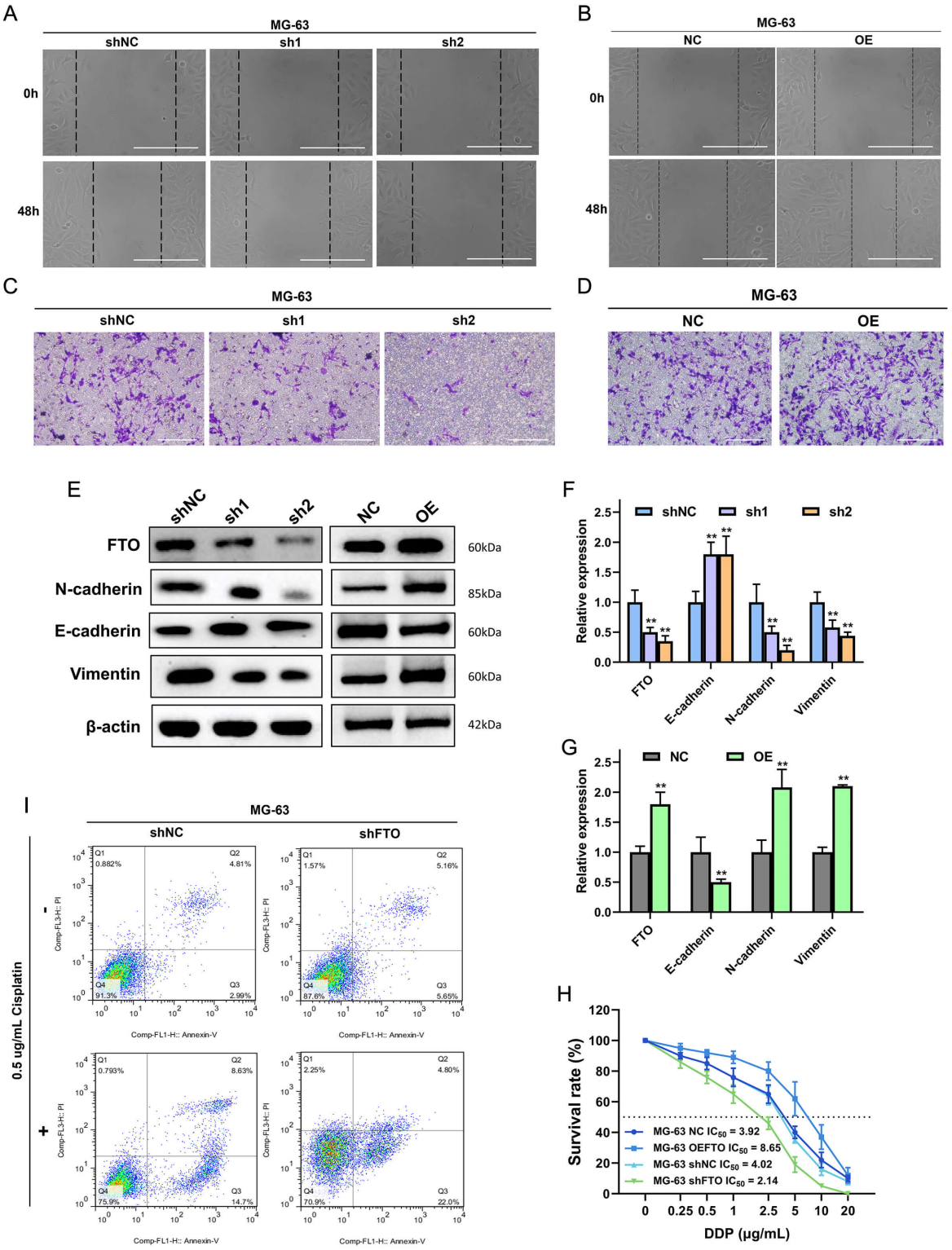


Fig. 3. FTO promotes osteosarcoma cell migration and reduces cisplatin sensitivity *in vitro*. (A,B) Wound healing assay in FTO knockdown (A) and overexpression (B) MG-63 cells. Scale bar, 200 μm. (C,D) Transwell migration assay in MG-63 cells with FTO knockdown (C) and overexpression (D). Scale bar, 200 μm. (E–G) Western blot showing epithelial-mesenchymal transition-related protein levels in FTO knockdown (E,F) and overexpression (E,G) MG-63 cells. β-actin was used as a reference. (H) CCK-8 assay determining the IC_{50} of cisplatin in FTO knockdown and overexpression MG-63 cells. The dashed line indicates 50% cell survival. (I) Flow cytometry analyses showing proportion of apoptotic cells in cisplatin-treated FTO knockdown MG-63 cells. $^{**}p < 0.01$.

IMR Press

ever, the precise molecular mechanism by which FTO regulates PI3K-Akt signaling remains to be elucidated. In summary, *FTO* promotes osteosarcoma proliferation and inhibits apoptosis.

To validate this, a wound-healing assay was performed using MG-63 cells, and the results showed that within 48 h, the wound-healing ratio in the *FTO* knockdown group was significantly lower than that in the control group. In contrast, *FTO* overexpression significantly accelerated the healing rate (Fig. 3A,B and **Supplementary Fig. 1E,F**). Additionally, the transwell assay showed that after *FTO* knockdown, the number of cells migrating to the lower chamber decreased significantly, whereas *FTO* overexpression increased cell migration to the lower chamber (Fig. 3C,D and **Supplementary Fig. 1G,H**). Subsequent western blot demonstrated that *FTO* knockdown significantly increased the expression of the epithelial marker E-cadherin while decreasing the expression of the mesenchymal markers N-cadherin and Vimentin. Conversely, *FTO* overexpression downregulated E-cadherin and upregulated N-cadherin and Vimentin levels (Fig. 3E–G). These findings indicate that *FTO* promotes osteosarcoma cell migration.

As a first-line chemotherapeutic agent for osteosarcoma, cisplatin sensitivity has consistently been a key area of research. The CCK-8 assay found varying sensitivity to cisplatin among osteosarcoma cell lines. Interestingly, HOS cells with high *FTO* expression exhibited a higher IC_{50}, while U-2OS cells with low *FTO* expression showed a relatively lower IC_{50}, suggesting *FTO* expression may affect cisplatin sensitivity (**Supplementary Fig. 1I**). To directly validate this, the IC_{50} values of cisplatin in genetically modified MG-63 cells were compared. FTO knockdown significantly reduced the IC_{50} compared to control cells, whereas FTO overexpression markedly increased the IC_{50} (Fig. 3H). Consistent with these results, flow cytometry confirmed that *FTO* knockdown increased cisplatin-induced apoptosis in MG-63 cells (Fig. 3I and **Supplementary Fig. 1J**). Taken together, these findings suggest that *FTO* reduces cisplatin sensitivity and may be related to osteosarcoma cisplatin resistance.

3.3 FTO Promotes Osteosarcoma Progression and Metastasis In Vivo

To validate the *in vivo* effects of *FTO* on osteosarcoma, a subcutaneous tumor-bearing model was established in nude mice using *FTO*-knockdown and overexpression in MG-63 cells. It was found that knocking down the *FTO* expression significantly reduced tumor growth rate. At the endpoint of the experiment, the mean tumor volume in the shFTO groups was significantly smaller than that in the shNC group (shNC: 1024.02 ± 109.93 mm^3; sh1: 567.29 ± 103.65 mm^3; sh2: 482.80 ± 114.79 mm^3) (Fig. 4A,B). And the tumor proliferative capacity was diminished according to tumor Ki67 staining (Fig. 4A,D). Conversely, FTO overexpression markedly accelerated tumor growth, resulting in a significantly larger tumor volume (NC: 1182.67 ± 192.27 mm^3; OE-FTO: 1619.45 ± 193.58 mm^3) (Fig. 4A,C), which was accompanied by increased Ki67 positivity (Fig. 4A,E). These results demonstrate that FTO promotes osteosarcoma tumor growth *in vivo*. The pulmonary metastasis model via tail vein injection suggested that *FTO* knockdown reduced the number and size of visible pulmonary nodules (Fig. 4F,G). Histological examination of H&E-stained lung sections confirmed the presence of tumor metastases and showed a significantly lower metastatic burden in the shFTO group (Fig. 4F and **Supplementary Fig. 1K**). Conversely, FTO overexpression markedly increased both surface nodule counts and metastatic burden (Fig. 4H,I and **Supplementary Fig. 1L**).

3.4 YAP Is a Downstream Target Gene of FTO

After exploring the *in vitro* and *in vivo* functions of *FTO* in osteosarcoma, it would be meaningful to investigate its downstream regulatory mechanisms. Thus, transcriptome sequencing was performed, and the heatmap showed 178 differentially expressed genes after *FTO* knockdown, of which 97 were significantly upregulated, and 81 were downregulated (Fig. 5A,B). KEGG pathway enrichment indicated that the differentially expressed genes were enriched in several signaling pathways, including the Hippo pathway, apoptosis-related pathway, Wnt pathway, and the hypoxia-response pathways (Fig. 5C). *YAP*, the core transcriptional factor of the Hippo pathway, exhibited a downregulated trend after *FTO* was knocked down in transcriptome sequencing, suggesting it might be a downstream target of *FTO*. Subsequent qPCR confirmed that *YAP* mRNA expression was significantly decreased following *FTO* knockdown (Fig. 5D). Western blot found that *YAP* protein levels showed the same trend as mRNA after *FTO* knockdown, and *FTO* overexpression significantly increased *YAP* protein levels (Fig. 5E, **Supplementary Fig. 2A,B**). Correlation analysis of gene expression using GEPIA showed a significant positive correlation between *FTO* and *YAP* expression (Fig. 5F). These results suggest *YAP* is a downstream gene of *FTO*.

Given that FTO functions as an m^6A demethylase, it was of importance to investigate whether *YAP* mRNA could be a direct substrate for FTO-mediated m^6A modification. Thus, SRAMP database, a sequence-based m^6A modification site predictor [21], was employed and multiple high-confidence m^6A modification sites on the *YAP* mRNA was identified (**Supplementary Fig. 2C** and **Supplementary Table 3**). Furthermore, by querying the RM2Target database, which integrates comprehensive RNA modification targeting data from public datasets [22], we found existing experimental evidence including CLIP-seq/eCLIP-seq data supporting the binding of FTO to *YAP* mRNA (**Supplementary Table 3**). To determine whether FTO directly interacts with *YAP* mRNA, RIP was performed

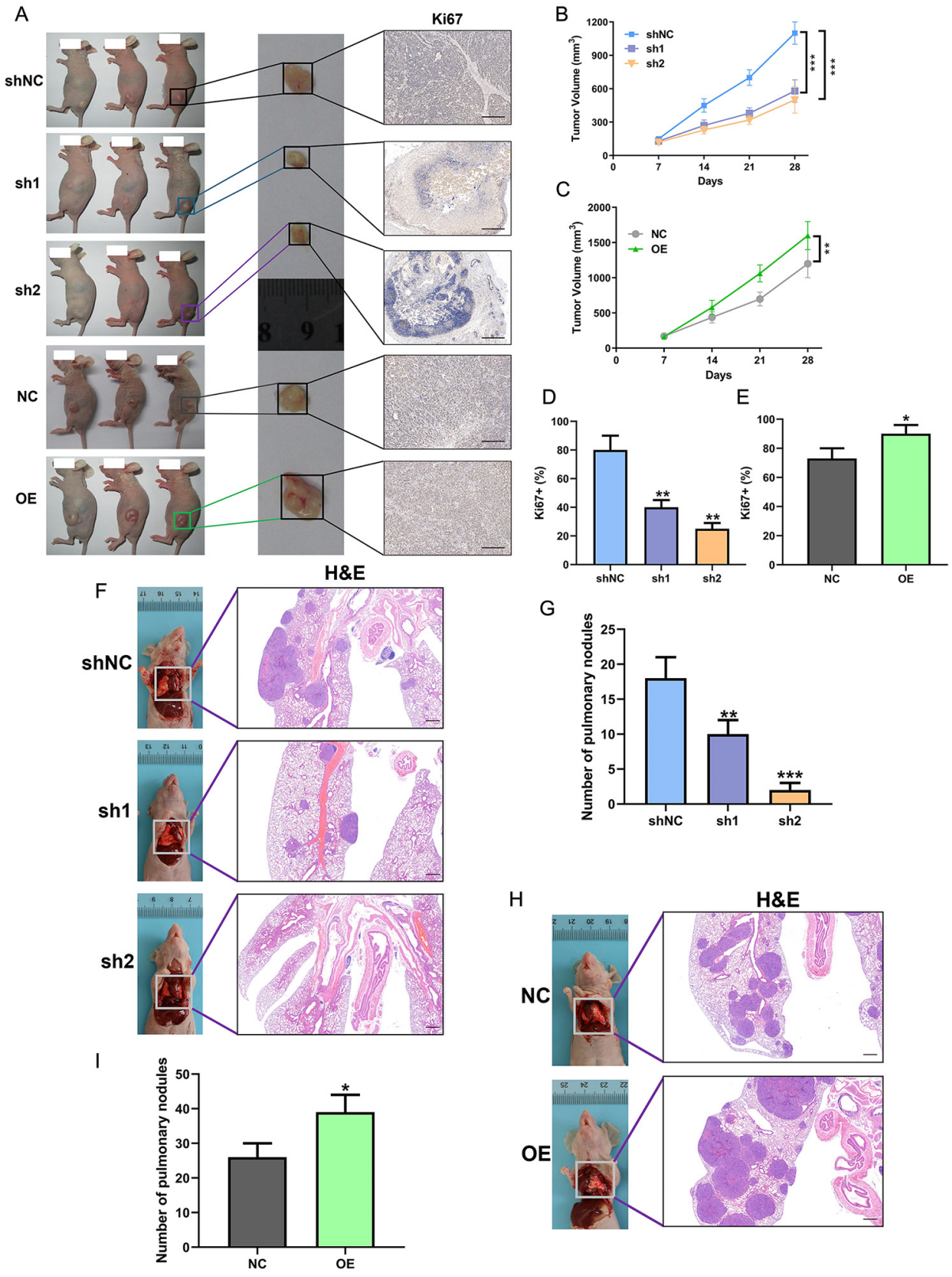


Fig. 4. FTO promotes osteosarcoma development and metastasis *in vivo*. (A) Subcutaneous xenograft tumors formed by FTO knockdown or overexpression MG-63 cells in nude mice. The gross tumor images and Ki67 staining were shown. Scale bar, 500 μm. (B–E) Tumor growth curves (B,C) and percentage of $Ki67^+$ cells (D,E) in FTO knockdown (B,D) and overexpression (C,E) groups. (F–I) Images and counts of pulmonary metastatic nodules of FTO knockdown (F,G) and overexpression (H,I) MG-63 cells. Scale bar, 500 μm. $^*p < 0.05$, $^{**}p < 0.01$, $^{***}p < 0.001$.

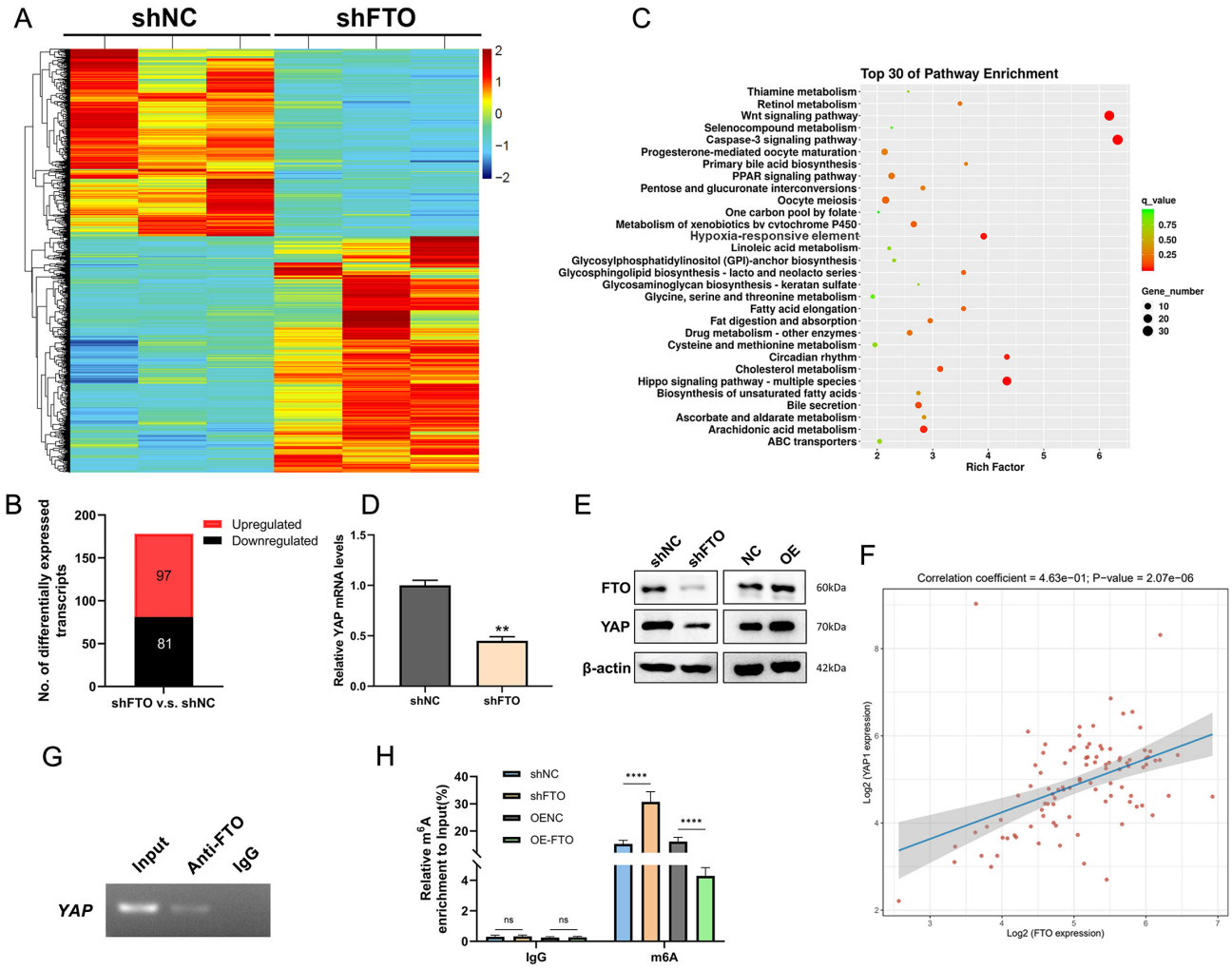


Fig. 5. Transcriptome sequencing-based analysis of FTO target genes. (A) Heatmap of differentially expressed genes from transcriptome sequencing of FTO knockdown vs. shNC MG-63 cells. (B) Number of differentially expressed genes identified. (C) KEGG pathway enrichment analysis of differentially expressed genes. (D) qPCR showing YAP expression in MG-63 cells after FTO knockdown. β-actin was used as a reference gene. (E) Western blot revealing YAP protein levels in FTO knockdown and overexpression MG-63 cells. β-actin was used as an internal reference. (F) Correlation analysis of FTO and YAP mRNA expression in osteosarcoma. (G) RIP-PCR showing the direct binding of FTO to YAP mRNA in MG-63 cells. IgG was used as a negative control. (H) MeRIP-qPCR revealing the m^{6}A enrichment levels of *YAP* mRNA in FTO knockdown and overexpression MG-63 cells. $^{**}p < 0.01$, $^{****}p < 0.0001$, ns, non-significant.

using an anti-FTO antibody. A clear PCR product corresponding to *YAP* mRNA was detected in the FTO-immunoprecipitated samples, whereas only an undetectable band was observed in the IgG control (Fig. 5G). Furthermore, the results of the MeRIP-qPCR experiments indicate that, compared with their respective control groups, FTO knockdown led to a significant increase in the m^{6}A abundance of YAP mRNA, while FTO overexpression resulted in a significant decrease (Fig. 5H). Collectively, bioinformatic predictions and results suggest that *YAP* is a downstream target of FTO, and its expression is regulated by FTO through an m^{6}A-dependent mechanism.

3.5 FTO Promotes Osteosarcoma Progression In Vitro via YAP

The expression analysis of *YAP* across multiple cancer types demonstrated inconsistent expression patterns (Fig. 6A). In osteosarcoma, *YAP* expression was significantly upregulated (Fig. 6B), consistent with *FTO* (Fig. 1B). Furthermore, high *YAP* expression was associated with a lower overall survival rate in patients with tumors (Fig. 6C). Combined with previous studies, these findings suggest that *YAP* plays an oncogenic role in osteosarcoma.

Given that *YAP* is a downstream target of *FTO*, it is important to clarify whether *FTO* promotes osteosarcoma via *YAP*. To validate this, cell line models for *FTO* knockdown combined with *YAP* overexpression, and *FTO*

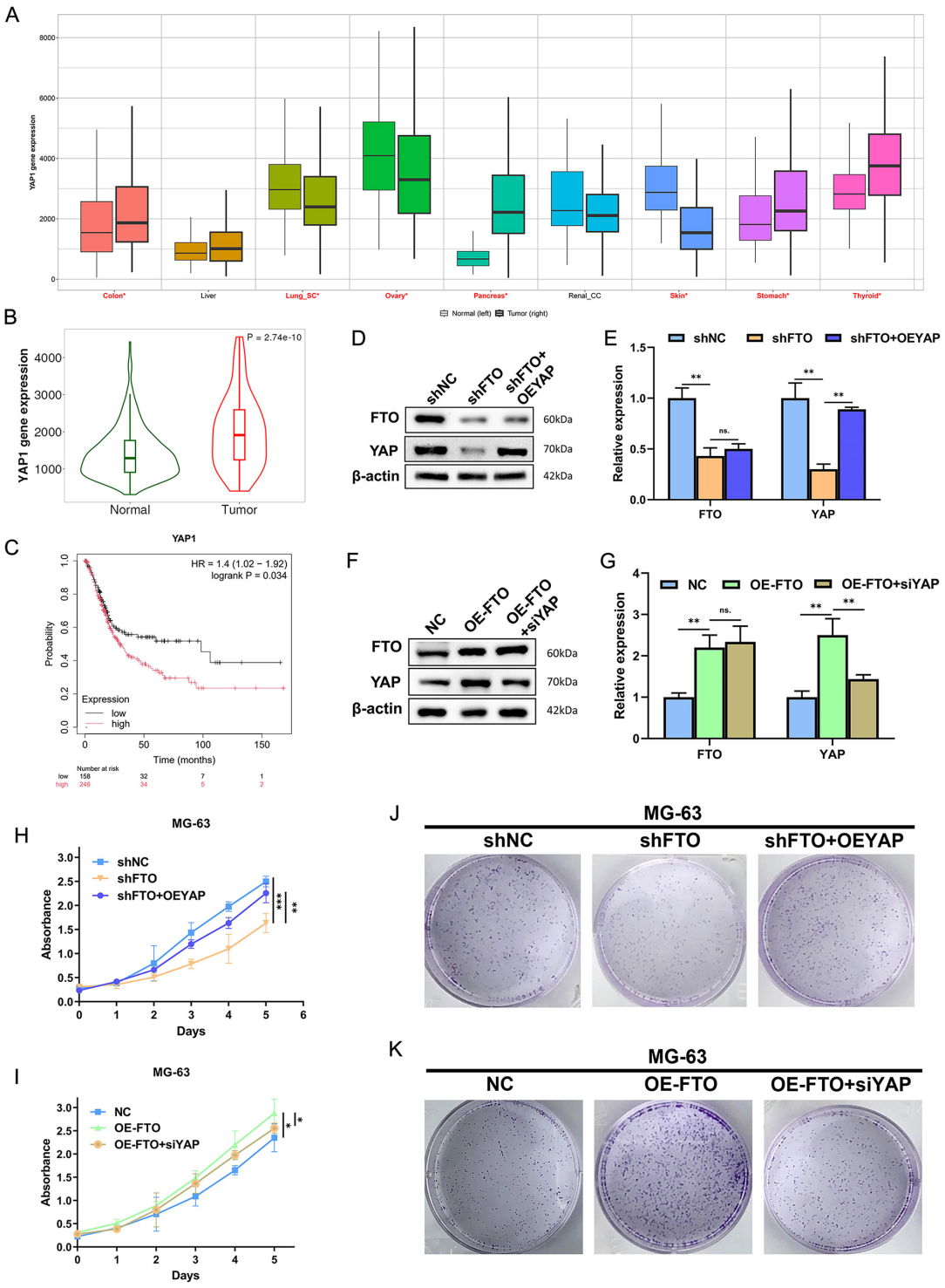


Fig. 6. YAP is a functional target of FTO in promoting osteosarcoma progression *in vitro*. (A) Pan-cancer analysis of YAP expression. Red labels indicate statistically significant differences. (B) Comparison of YAP expression in osteosarcoma vs. normal bone tissue. (C) Kaplan-Meier survival analysis of YAP expression in cancer patients. (D,E) Western blot showing FTO and YAP protein levels in shNC, shFTO, and shFTO + OEYAP MG-63 cells. β-actin was used as a reference. (F,G) Western blot exhibiting FTO and YAP protein levels in MG-63 cells of NC, OEFTO, and OEFTO + siYAP groups. β-actin was used as an internal reference. (H,I) CCK-8 assay showing the rescue effects of YAP overexpression on FTO knockdown-induced proliferation changes (H) and YAP knockdown on FTO overexpression-induced proliferation changes (I) in MG-63 cells. (J,K) Colony formation assay showing the rescue effects of YAP overexpression on FTO knockdown-induced proliferation changes (J) and YAP knockdown on FTO overexpression-induced proliferation changes (K) in MG-63 cells. $^{*}p < 0.05$, $^{**}p < 0.01$, $^{***}p < 0.001$, ns, non-significant.

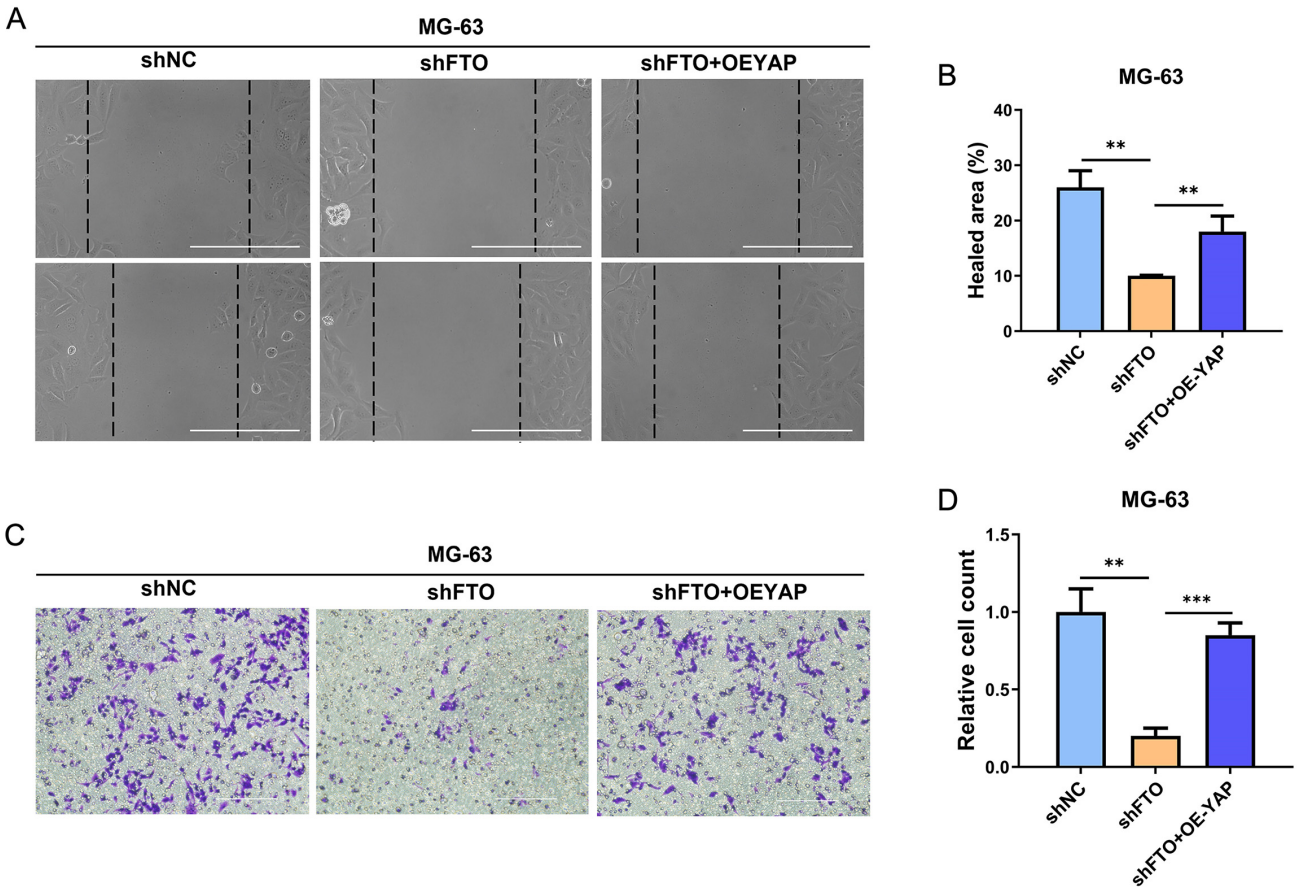


Fig. 7. FTO promotes MG-63 cell migration through YAP *in vitro*. (A,B) Wound healing assay showing the rescue effect of YAP overexpression on FTO knockdown-induced migration impairment in MG-63 cells. Scale bar, 200 µm. (C,D) Transwell migration assay across experimental groups. Scale bar, 200 µm. $^{**}p < 0.01$, $^{***}p < 0.001$.

overexpression combined with *YAP* knockdown were established. Western blot confirmed the successful construction of these cell lines and indicated that modulated *FTO* significantly altered *YAP* expression, while changes in *YAP* expression did not markedly affect *FTO* levels (Fig. 6D–G). CCK-8 assay revealed that *YAP* overexpression could partially rescue the proliferation inhibition caused by *FTO* knockdown, while *YAP* knockdown suppressed the tumor proliferation promotion induced by *FTO* overexpression (Fig. 6H,I). And plate colony formation assay further supported these findings (Fig. 6J,K and **Supplementary Fig. 2D,E**). Wound-healing and Transwell assays showed that the impaired cell-migration caused by *FTO* knockdown could be partially rescued by *YAP* overexpression (Fig. 7A–D). Statistical analysis confirmed that the rescue group remained significantly different from the control group ($p < 0.05$), indicating partial rescue. In summary, these results demonstrate that *FTO* promotes osteosarcoma cell proliferation and migration of osteosarcoma cells *in vitro* through *YAP*.

3.6 FTO Promotes Tumor Progression In Vivo Through YAP

Since *FTO* promotes osteosarcoma progression *in vitro* via *YAP* and drives tumor progression *in vivo*, it is necessary to elucidate YAP's role in *FTO*-mediated *in vivo* cancer promotion. Hence, subcutaneous tumorigenesis experiments were performed, and the results showed that *FTO* knockdown inhibited tumor growth, an effect counteracted by *YAP* overexpression (shNC: 978.19 ± 97.42 mm^3; shFTO: 512.38 ± 105.27 mm^3; shFTO + OEYAP: 837.88 ± 116.69 mm^3) (Fig. 8A,B). Additionally, in the tail vein injection-established lung metastasis model, *FTO* knockdown reduced the number of pulmonary metastatic nodules, alleviating the tumor metastasis burden, and *YAP* overexpression significantly attenuated this inhibitory effect (Fig. 8C,D and **Supplementary Fig. 2F**). In summary, as a downstream target of *FTO*, *YAP* mediates the tumor-promoting effects of FTO *in vivo*.

4. Discussion

As one of the most abundant epigenetic modifications in eukaryotic mRNA, m^6A is dynamically regulated by various proteins and profoundly influences tumor initiation and

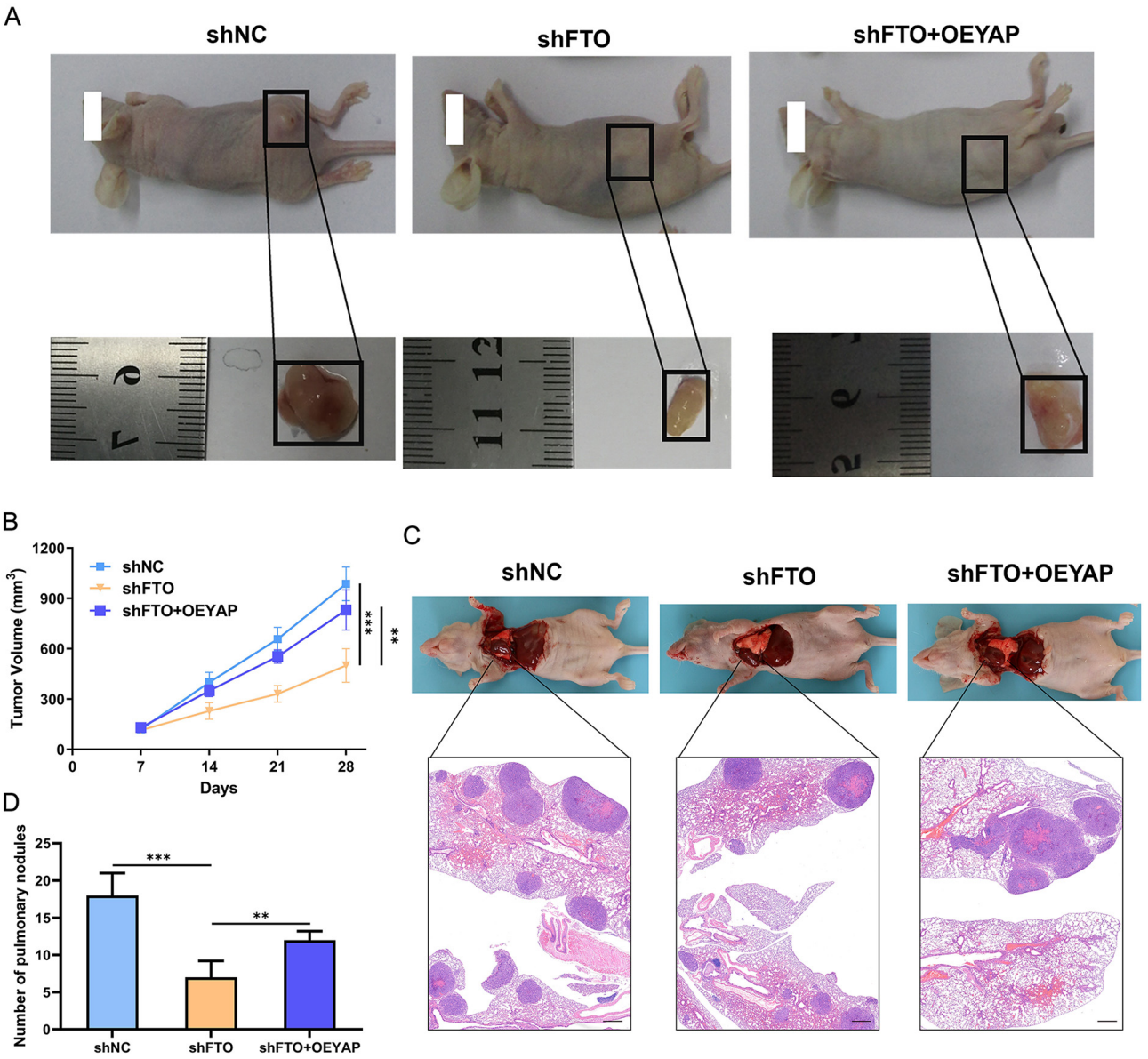


Fig. 8. FTO promotes tumor progression *in vivo* via YAP. (A,B) Rescue effect of YAP overexpression on FTO knockdown-induced suppression of MG-63 tumor growth. (C,D) Rescue of the reduction in pulmonary metastatic nodule by YAP overexpression in FTO-knockdown MG-63 cells. Scale bar, 200 μm. $^{**}p < 0.01$, $^{***}p < 0.001$.

progression [23,24,25,26]. As a key m^{6}A demethylase, *FTO* has been demonstrated to be overexpressed and exert oncogenic functions in multiple malignancies, including leukemia [27] and melanoma [28]. However, its specific role and downstream targets in osteosarcoma remain incompletely elucidated.

In this study, through bioinformatic analysis and *in vitro* experiments, we confirmed that *FTO* expression is significantly upregulated in osteosarcoma. Gain- and loss-of-function experiments demonstrated that *FTO* promotes osteosarcoma cell proliferation and migration. Subcutaneous xenograft and tail vein injection metastasis models further validated *FTO*'s role in driving *in vivo* osteosarcoma growth and metastasis. Cisplatin is one of the first-line chemotherapeutic drugs for osteosarcoma; however, variable sensitivity and drug resistance pose major challenges in clinical treatment. The *in vitro* experiments revealed that differences in *FTO* expression levels correlate with variable cisplatin sensitivity among osteosarcoma cell lines, and that modulation of *FTO* expression alters their sensitivity to cisplatin. These findings establish the functional role of *FTO* in osteosarcoma.

Moreover, we further investigated the underlying mechanism. Through bioinformatic analysis and transcriptome sequencing, we identified *YAP* as a key downstream target of *FTO*. *YAP* is a critical effector of the Hippo signaling pathway. Bioinformatic analysis indicated that *YAP* exhibits diverse expression patterns across different can-

cers. In osteosarcoma, *YAP* expression shows an upregulation trend consistent with that of *FTO*. Previous studies have shown that *YAP* plays a tumor-promoting role in osteosarcoma. By generating cell lines with combined modulation of *FTO* and *YAP*, we demonstrated that *YAP* is the key downstream effector mediating the pro-proliferative and pro-metastatic effects of *FTO* in osteosarcoma, both *in vitro* and *in vivo*. Furthermore, *FTO* modulates cisplatin sensitivity in osteosarcoma via *YAP*. These findings reveal the *FTO-YAP* regulatory axis, providing deeper insights into the specific mechanisms by which *FTO* drives osteosarcoma progression. Notably, the *FTO/YAP* regulatory axis has been previously implicated in chemoresistance in other cancer types. The present study extends this mechanistic framework to osteosarcoma, demonstrating for the first time that FTO modulates cisplatin sensitivity through a *YAP*-dependent pathway. These findings suggest that targeting the *FTO/YAP* axis may represent a novel therapeutic strategy to overcome cisplatin resistance in osteosarcoma.

In summary, this study demonstrates the role of *FTO* in osteosarcoma progression and cisplatin sensitivity, revealing that it exerts its oncogenic functions through its downstream target gene *YAP*. These findings provide a theoretical foundation for identifying potential therapeutic targets in osteosarcoma and offer insights for developing novel treatment strategies.

5. Limitations

It should be noted that this study has certain limitations. The conclusion regarding FTO's specific overexpression in osteosarcoma is primarily based on bioinformatic analysis. Future studies incorporating paired normal bone tissue would help strengthen the clinical conclusions. For the reason that MG-63 has moderate FTO expression to facilitate bidirectional modulation, it was chosen for mechanistic experiments, and extension to additional cell lines would be beneficial. In addition, the observed changes in PI3K-Akt phosphorylation and the cisplatin response were assessed through correlative and short-term sensitivity assays, respectively. Further experiments are needed to explore the underlying causal mechanisms and long-term resistance. Finally, the partial rescue by YAP suggests that other pathways may also contribute to the effects of FTO, which could be investigated in subsequent studies.

6. Conclusions

FTO is prominently expressed in osteosarcoma, promoting disease progression and diminishing sensitivity to cisplatin. *YAP*, a downstream effector of *FTO*, is also highly expressed in osteosarcoma and plays a mediating role in the oncogenic effects.

Abbreviations

AML, acute myeloid leukemia; FTO, fat mass and obesity-associated protein; IHC, immunohistochemistry; m^6A, N6-methyladenosine; YAP, Yes-associated protein.

Availability of Data and Materials

The sequencing data have been submitted to the Gene Expression Omnibus (GEO) database, and the accession number is GSE341587. All other data are available from the corresponding authors upon reasonable request.

Author Contributions

ZS: Conceptualization, Investigation, Formal Analysis, Writing – original draft. FL: Visualization, Writing – original draft. ZC: Investigation, Validation. YZ: Resources, Data acquisition, Investigation. XD: Supervision, Formal Analysis, Investigation. HW: Writing – review and editing, Funding acquisition, Investigation, Formal Analysis. All authors contributed to editorial changes in the manuscript. All authors read and approved the final manuscript. All authors have participated sufficiently in the work and agreed to be accountable for all aspects of the work.

Ethics Approval and Consent to Participate

The human osteosarcoma tissue microarray used in this study was commercially obtained from Xi'an Zhongke Guanghua Bioaitech Co., Ltd. (L714901, Xi'an, Shaanxi, China). According to the provider, all human tissue samples were collected with informed consent from the donors or their relatives, in strict accordance with the Declaration of Helsinki. All patient information was fully de-identified and anonymized. The Ethics Committee of the Second Affiliated Hospital of Xi'an Jiaotong University confirmed that no additional ethical approval was required for the use of these commercially available, anonymized human tissue samples.

All animal experiments were performed in accordance with the ARRIVE guidelines and the relevant national standard GB/T 35892-2018 (Laboratory animal—Guideline for ethical review of animal welfare). All animal procedures were conducted in accordance with the Guide for the Care and Use of Laboratory Animals and were approved by the Institutional Animal Care and Use Committee (IACUC) of the Laboratory Animal Research Center of Xi'an Jiaotong University, under approval number: XJTUAE20253836.

Acknowledgment

Not applicable.

Funding

This work was supported by the Key Research Project of Shaanxi Province (No.2025SF-YBXM-453).

Conflicts of Interest

The authors declare no conflicts of interest.

Supplementary Material

Supplementary material associated with this article can be found, in the online version, at https://doi.org/10.31083/FBL53084.

References

[1] Greenwood AC, Arora RD, Shaikh H. Osteosarcoma (osteogenic sarcoma). StatPearls [Internet]. 2024. Available at: https://www.ncbi.nlm.nih.gov/books/NBK563177/ (Accessed: 17 December 2025)

[2] Garcia-Ortega DY, Cabrera-Nieto SA, Caro-Sánchez HS, Cruz-Ramos M. An overview of resistance to chemotherapy in osteosarcoma and future perspectives. Cancer Drug Resistance (Alhambra, Calif.). 2022; 5: 762–793. https://doi.org/10.20517/cdr.2022.18

[3] An L, Zhuang Y, Sun H. NGF/BDNF-Trk/p75NTR signaling in osteosarcoma immunity: biomarkers and therapeutic opportunities. Frontiers in Immunology. 2025; 16: 1719012. https://doi.org/10.3389/fimmu.2025.1719012

[4] Zhu Y, Li W, Qiu Y, Deng Z, Li Y, Chen H, et al. HP1 enhances radio- and chemotherapy resistance in osteosarcoma via PARP1-dependent transcriptional repression and HR repair. Cancer Letters. 2026; 639: 218213. https://doi.org/10.1016/j.canlet.2025.218213

[5] Zhao X, Guan S. Epitranscriptomic control of cancer immunity and therapy resistance. Frontiers in Immunology. 2025; 16: 1706557. https://doi.org/10.3389/fimmu.2025.1706557

[6] Luo H, Kharas MG, Jaffrey SR. N^6-Methyladenosine: an RNA modification as a central regulator of cancer. Nature Reviews. Cancer. 2026; 26: 118–136. https://doi.org/10.1038/s41568-025-00889-6

[7] Kim H, Lee YS, Kim SM, Jang S, Choi H, Lee JW, et al. RNA demethylation by FTO stabilizes the FOXJ1 mRNA for proper motile ciliogenesis. Developmental Cell. 2021; 56: 1118–1130.e6. https://doi.org/10.1016/j.devcel.2021.03.006

[8] Deng H, Liu Q, Gong Y, Qiu Y. Regulation of m6A methylation in the immune microenvironment in the development of diabetes mellitus. Journal of Translational Medicine. 2025; 23: 1308. https://doi.org/10.1186/s12967-025-07331-3

[9] Zhao F, Zou Z, Liu Z, Wang J, Wu Y, Zhang J, et al. A lysine-restricted diet ameliorates obesity via enrichment of Parabacteroides goldsteinii and 1,4-methylimidazoleacetic acid. Nature Communications. 2025; 16: 9953. https://doi.org/10.1038/s41467-025-64892-z

[10] Saad AAA, Ge L, Wang H, Xia Y, Li J, Qiao S, et al. Combination of FTO and BTK inhibitors synergistically suppresses the malignancy of breast cancer cells. International Journal of Biological Sciences. 2025; 21: 7063–7085. https://doi.org/10.7150/ijbs.117999

[11] Zhang S, Zhao S, Qi Y, Li B, Wang H, Pan Z, et al. SPI1-induced downregulation of FTO promotes GBM progression by regulating pri-miR-10a processing in an m6A-dependent manner. Molecular Therapy. Nucleic Acids. 2022; 27: 699–717. https://doi.org/10.1016/j.omtn.2021.12.035

[12] Zou D, Dong L, Li C, Yin Z, Rao S, Zhou Q. The m^6A eraser FTO facilitates proliferation and migration of human cervical cancer cells. Cancer Cell International. 2019; 19: 321. https://doi.org/10.1186/s12935-019-1045-1

[13] Liao Q, Shi H, Yang J, Ge S, Jia R, Song X, et al. FTO elicits tumor neovascularization in cancer-associated fibroblasts through eliminating m^6A modifications of multiple pro-angiogenic factors. Cancer Letters. 2024; 592: 216911. https://doi.org/10.1016/j.canlet.2024.216911

[14] Bala R, Madaan R, Bedi O, Singh A, Taneja A, Dwivedi R, et al. Targeting the Hippo/YAP Pathway: A Promising Approach for Cancer Therapy and Beyond. MedComm (2020). 2025; 6: e70338. https://doi.org/10.1002/mco2.70338

[15] Kim HS, Nam JS. The multifaceted role of YAP in the tumor microenvironment and its therapeutic implications in cancer. Experimental & Molecular Medicine. 2025; 57: 2201–2213. https://doi.org/10.1038/s12276-025-01551-9

[16] Zhu T, Song H, Yu Y, Huang W, Zhang Y, Zhang Z, et al. CPE/HYOU1 axis-activated Hippo-YAP signaling pathway suppresses PANoptosis to facilitate osteosarcoma progression. Cancer Letters. 2026; 639: 218121. https://doi.org/10.1016/j.canlet.2025.218121

[17] Chan L, Wang W, Yeung W, Deng Y, Yuan Y, Chen Y, et al. Hedgehog signaling induces osteosarcoma development through Yap1 and H19 overexpression. Oncogene. 2014; 33: 4857–4866. https://doi.org/10.1038/onc.2013.433

[18] Wang R, Cheng F, Yang X. FTO attenuates the cytotoxicity of cisplatin in KGN granulosa cell-like tumour cells by regulating the Hippo/YAP1 signalling pathway. Journal of Ovarian Research. 2024; 17: 62. https://doi.org/10.1186/s13048-024-01385-5

[19] Bartha Á, Győrffy B. TNMplot.com: A Web Tool for the Comparison of Gene Expression in Normal, Tumor and Metastatic Tissues. International Journal of Molecular Sciences. 2021; 22: 2622. https://doi.org/10.3390/ijms22052622

[20] Tang Z, Kang B, Li C. GEPIA2: an enhanced web server for large-scale expression profiling and interactive analysis. Nucleic Acids Research. 2019; 47: W556–W560. https://doi.org/10.1093/nar/gkz430

[21] Zhou Y, Zeng P, Li YH, Zhang Z, Cui Q. SRAMP: prediction of mammalian N6-methyladenosine (m6A) sites based on sequence-derived features. Nucleic Acids Research. 2016; 44: e91. https://doi.org/10.1093/nar/gkw104

[22] Bao X, Jiang Q, Chen W, Li H, Li X, Zuo X, et al. RM2Target v2.0: an updated database for the target genes of writers, erasers, and readers of RNA modifications. Nucleic Acids Research. 2026; 54: D279–D290. https://doi.org/10.1093/nar/gkaf1206

[23] Zhou H, Chen H, Liu W, Liang C, Wang S, Yuan K, et al. Targeting of the m^6A eraser ALKBH5 suppresses stemness and chemoresistance of colorectal cancer. Nature Communications. 2025; 17: 803. https://doi.org/10.1038/s41467-025-67502-0

[24] Chen Y, Dai S, Zhuang L, Cai W, Chen H, Zhao J, et al. NRAV promotes HCC stemness via the m6A-regulated let-7c-5p/LIN28B axis. Cancer Gene Therapy. 2026; 33: 171–185. https://doi.org/10.1038/s41417-025-00995-5

[25] Liu H, Tan S, Zhao Z, Tang X, Li Z, Qi J. METTL3/YTHDF1 stabilizes MTCH2 mRNA to regulate ferroptosis in glioma cells. Frontiers in Bioscience (Landmark Edition). 2025; 30: 25718. https://doi.org/10.31083/FBL25718

[26] Zhu L, Li X, Wang W. METTL3-driven m6A modification of Cpt1a gene in high fat diet related liver cancer tumor macrophages facilitates type II macrophage differentiation. Frontiers in Bioscience (Landmark Edition). 2025; 30: 36971. https://doi.org/10.31083/FBL36971

[27] Li X, Yang Z, Huang S, Wang J, Wang X, Liang Y, et al. FTO inhibition represses B-cell acute lymphoblastic leukemia progression by inducing nucleolar stress and mitochondrial dysfunction. Free Radical Biology & Medicine. 2025; 238: 507–521. https://doi.org/10.1016/j.freeradbiomed.2025.07.004

[28] Yang S, Wei J, Cui YH, Park G, Shah P, Deng Y, et al. m^6A mRNA demethylase FTO regulates melanoma tumorigenicity and response to anti-PD-1 blockade. Nature Communications. 2019; 10: 2782. https://doi.org/10.1038/s41467-019-10669-0